

Structure and dynamics of *l*-Ge: Neutron scattering experiments and *ab initio* molecular dynamics simulations

Virginie Hugouvieux*

Laboratoire des Colloïdes, Verres et Nanomatériaux, CNRS, UMR 5587,
Université Montpellier 2, 34095 Montpellier Cedex 5, France and
Institut Laue-Langevin, BP 156, 38042 Grenoble cedex 9, France

Emmanuel Farhi and Mark R. Johnson

Institut Laue-Langevin, BP 156, 38042 Grenoble cedex 9, France

Fanni Juranyi

Laboratory for Neutron Scattering, PSI, 5232 Villigen, Switzerland

Philippe Bourges

Laboratoire Léon Brillouin, CEA Saclay, 91191 Gif sur Yvette cedex, France

Walter Kob

Laboratoire des Colloïdes, Verres et Nanomatériaux, CNRS, UMR 5587,
Université Montpellier 2, 34095 Montpellier Cedex 5, France

We report the first measurements of the dynamics of liquid germanium (*l*-Ge) by quasi-elastic neutron scattering on time-of-flight and triple-axis spectrometers. These results are compared with simulation data of the structure and dynamics of *l*-Ge which have been obtained with *ab initio* density functional theory methods. The simulations accurately reproduce previous results from elastic and inelastic scattering experiments, as well as the q -dependence of the width of the quasi-elastic signal of the new experimental data. In order to understand some special features of the structure of the liquid we have also simulated amorphous Ge. Overall we find that the atomistic model represents accurately the average structure of real *l*-Ge as well as the time dependent structural fluctuations. The new quasi-elastic neutron scattering data allows us to investigate to what extent simple theoretical models can be used to describe diffusion in *l*-Ge.

PACS numbers: 61.25.-f, 61.12.Ex, 61.20.Ja, 61.20.Lc

I. INTRODUCTION

The investigation of the structure of the condensed phases of germanium is of importance for fundamental science since this material exhibits polymorphism in the solid state and pronounced changes in density and bonding upon melting. Research in this field is also relevant to several applied physics problems and semiconductor technology.

In its solid phase germanium shows a large degree of polymorphism. In its stable crystalline phase at ambient pressure, the crystal has a diamond structure in which each Ge atom is surrounded by four covalently bonded first neighbors in a tetrahedral formation. This phase of Ge has a very low density with respect to a close-packed structure and is semiconducting. Upon application of pressure, the tetrahedrally bonded network is disrupted and the number of neighbors and the density increase. Around 100 kbar, a phase transition to the metallic β -tin (or white-tin) structure occurs and at even higher pressures an hexagonal phase and a close-packed phase are found¹.

At standard pressure the melting temperature of crystalline Ge is $T_m = 1210.4$ K. At the melting transition the tetrahedral network is disrupted and the average co-

ordination number increases from 4 to about 7, which is still low compared to other liquid metals which typically have coordination number between 9 and 12. Liquid germanium is metallic². Germanium can also be produced in an amorphous phase in which distorted tetrahedra are connected in a continuous random network with defects. Amorphous germanium is semiconducting.

Experimental investigations of the density and bonding changes in different phases of germanium are numerous, using both X-ray^{3,4,5} and neutron diffraction^{6,7,8,9,10} techniques. The static structure factor shows features that differ from those found in simple liquids: The first diffraction maximum is unusually low and has a shoulder on its high momentum transfer side. Thus a hard-sphere model does not seem to be appropriate for describing the arrangement of atoms in *l*-Ge and several models have been proposed based on the short-range order found in white-tin (also called β -tin)⁴, on the coexistence of randomly distributed, molten metal-like atomic arrangement and covalent crystal-like atomic arrangement⁵, on a mixture of fourfold and highly coordinated metallic arrangements⁸ or on a quasicrystalline model of *l*-Ge⁶. However none of these accounts for all of the structural features of *l*-Ge.

In order to investigate the dynamics of *l*-Ge, Hosokawa

and co-workers¹¹ used inelastic X-ray scattering to measure the spectra for momentum transfers q from 0.2 to 2.8 \AA^{-1} . The phonon dispersion curve extracted from the low q spectra matches the hydrodynamic sound velocity¹². The study of the relationship between $S(q)$ and Γ_q , the half width of $S(q, \omega)$ at half maximum, shows that at higher q the measured spectral width cannot be described by the relationship given by de Gennes for simple dense fluids¹³ nor the expression for spectra of dense hard-sphere fluids given by Cohen and co-workers¹⁴. According to Hosokawa *et al.*¹¹, this discrepancy supports the view that neither the structure nor the dynamics of l -Ge can be described using a single pair interaction. However, Ashcroft¹⁵ proposed a cluster model with transient covalent structures in the liquid which seems to be consistent with the experimental results. In this model, the first maximum in $S(q)$ reflects the inter-cluster correlation while the shoulder on the high q side and the remaining oscillations are associated with the atom-atom contributions. Regarding the experimental results on the dynamics, Hosokawa *et al.* put forward the idea that the narrowing of the quasi-elastic line at the position of the maximum in $S(q)$, followed by an increase of Γ_q at q values that correspond to the location of the shoulder in $S(q)$, indicates that the covalent structures are diffusing slowly while individual atoms are subject to rapid translational motion.

Also on the theoretical side, much effort has been devoted to modeling and reproducing both structural and dynamic features of l -Ge. In 1985, Stillinger and Weber proposed a model potential function comprising both two- and three-atom contributions to describe the interactions in solid and liquid states of Si¹⁶. Molecular dynamics simulations of l -Si using this potential give structural properties in good agreement with the measurements. Subsequently this potential was also used for simulating amorphous germanium¹⁷. Later on the potential devised for l -Si was used with a different set of parameters which were obtained by fitting crystalline as well as liquid Ge phases¹⁸, the corresponding static structure factors and pair correlation functions therefore being in good agreement with the experimental results. However, it was found that the computed diffusion coefficient is larger than the experimental values by a factor of 2.

There have also been a number of *ab initio* molecular dynamics (AIMD) simulations of l -Ge, starting in 1993 with the work of Kresse and Hafner who found a quite good agreement between simulated and experimental pair correlation functions and electronic densities of states¹⁹. Subsequently they extended their study to the liquid metal-amorphous semiconductor transition²⁰. Their results for the pair correlation function and the static structure factor are in good agreement with experimental measurements for the amorphous phase. According to these authors, the results for the liquid indicate a broad homogeneous distribution of local bonding configurations and show that both classes of models proposed earlier (mixture of fourfold coordinated and

highly coordinated metallic arrangements⁸ and both sixfold coordinated and metallic arrangements⁴) are unrealistic. The simulation of supercooled and amorphous Ge shows the increase of the local tetrahedral order with decreasing temperature. The self-diffusion coefficient extracted from the simulated trajectory close to the melting point, $D = 1.0 \cdot 10^{-4} \text{ cm}^2/\text{s}$, is in good agreement with the measured value. Similar results about the structure and diffusion of l -Ge were found by Takeuchi and Garzón²¹ using the *ab initio* Car-Parrinello molecular-dynamics scheme²². A further study was performed by Godlevsky *et al.*²³ which yielded similar results for both the structure factor and the pair correlation function. Kulkarni and collaborators performed similar simulations and studied the influence of the temperature between 1250 K and 2000 K on the structural properties of the liquid²⁴. These simulations show that liquid Ge is a good metal but has some special short-range order arising from residual covalent bonding. Only at the highest temperatures, l -Ge seems to evolve toward a more conventional close-packed liquid metal. Calculations of the dynamic structure factor from an *ab initio* MD simulation were performed by Chai and co-workers²⁵. They show good agreement with the experimental data, although the statistical noise due to the small number of atoms (64) is rather large and has to be convoluted with a Gaussian of width 2.5 meV representing the experimental resolution function.

As can be seen from these experimental and theoretical studies, experimental investigations of l -Ge are presently not able to determine the microscopic, atomic arrangements in the liquid, but the experiments provide the data which is needed to validate theoretical models and simulations. In this paper, we present a new study of liquid germanium using both quasi-elastic neutron scattering (QENS) experiments and AIMD simulations. The QENS technique provides much clearer insight into diffusive dynamics than inelastic X-ray scattering in an intermediate q range due to the higher resolution and approximately Gaussian lineshape of the spectrometer resolution function. The QENS signal is typically most prominent at the q -range around the first sharp diffraction peak. QENS data therefore relates directly to local structural fluctuations on a length scale which is most relevant to the ongoing discussion about the structure of l -Ge. Section II presents details and results of the QENS measurements. Section III is dedicated to the *ab initio* simulations of the structure and dynamics of l -Ge and to the comparison with new and existing experimental results and in Section IV we summarize and conclude the present work.

II. NEUTRON SCATTERING STUDY OF l -Ge

QENS measurements on l -Ge were performed on cold neutron, time-of-flight (Focus at the Swiss spallation neutron source SINQ, PSI, Switzerland^{26,27,28}) and triple-axis (4F1 at Laboratoire Léon Brillouin, France²⁹) spec-

trometers. Note that due to the high sound velocity, $c_s = 2682 \text{ m/s}^{12}$, the acoustic phonon of l -Ge could not be measured.

A. Sample preparation and environment

Solid Ge samples were obtained either as a powder (obtained commercially with a purity of 99.99% in weight) or as pure solid pieces (less sensitive to oxidation and higher packing factor). Solid Ge was inserted into a cylindrical cell (6 mm in diameter) made of vitreous silica which was then sealed under vacuum. Sample preparation was performed either under nitrogen atmosphere or vacuum, in order to avoid contamination of dioxygen (which would lead to formation of GeO or GeO₂ at high temperatures). The silica cell was suspended from the end of the sample stick in a niobium envelope. The melting temperature of l -Ge is $T_m = 1210.4 \text{ K}$. During the neutron scattering experiments, Ge was heated in standard furnaces. After melting, the height of the sample was between 2 and 5 cm, depending on the initial solid form of Ge.

B. Experimental setup and data analysis

In both experiments, the sample temperature was comprised between 1260 K and 1400 K, with a sample of 6 mm in diameter.

On Focus, the measurements were performed at incident wavelengths of 3 Å and 4 Å. Momentum transfer ranges from 0.35 to 3.8 Å⁻¹ at $\lambda_i = 3 \text{ Å}$. Background measurements with comparable statistics were performed at both wavelengths for the furnace, empty sample cell and niobium envelope. The instrument resolution function was determined using a cylindrical vanadium sample of diameter 10 mm. The elastic energy resolution at incident wavelength of 3 Å and 4 Å was of the order of 500 μeV and 200 μeV , respectively. The data were processed with standard software at the instrument (NATHAN).

On 4F1 constant q scans were performed between $q = 0.3 \text{ Å}^{-1}$ and $q = 3.9 \text{ Å}^{-1}$, although the QENS signal could only be measured unambiguously for $q > 1.5 \text{ Å}^{-1}$. The data were processed with the standard 4F1 program.

C. Experimental results

The background signal was almost as strong as the signal from l -Ge. A slight misalignment between the sample and empty cell measurements meant that the data around the elastic peak had to be discarded. The difference spectra were fitted using a single Lorentzian for each q (see Fig. 1 for Focus results). The QENS intensity increases and the width decreases as q approaches 2.5 Å⁻¹. The triple-axis measurements give similar results (see Fig. 2). The evolution of the QENS signal

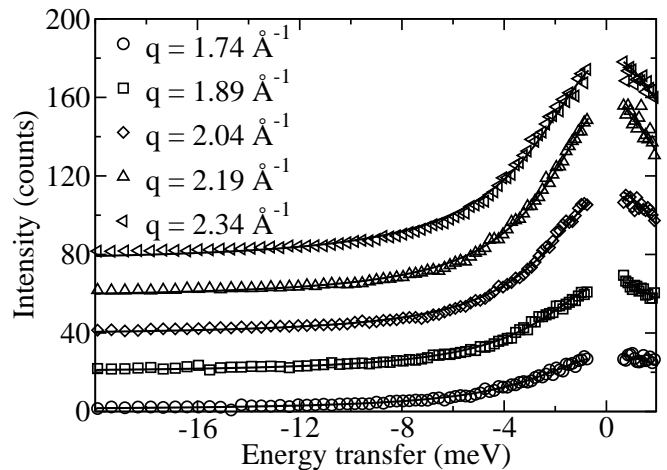


FIG. 1: Time-of-flight measurements of $S(q, \omega)$ for l -Ge at different q values ($\lambda_i = 3 \text{ Å}$; $T = 1260 \text{ K}$); different spectra are shifted vertically by 20 counts. The solid lines show the fitted Lorentzians.

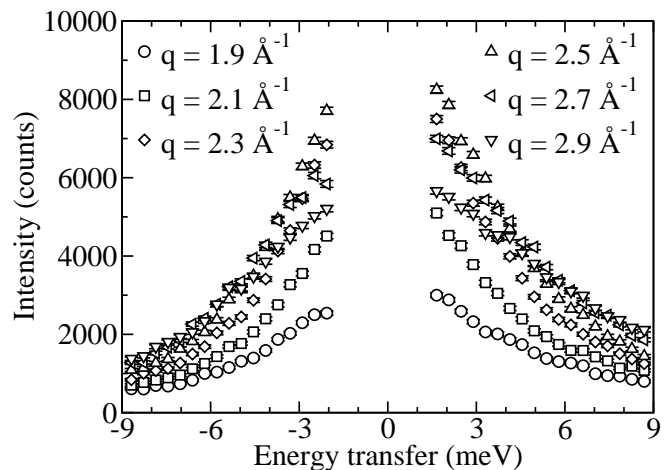


FIG. 2: Triple-axis measurements of $S(q, \omega)$ for l -Ge at different q values around the position of the first maximum in $S(q)$ ($k_f = 2.662 \text{ Å}^{-1}$, $T = 1300 \text{ K}$).

with q will be discussed below with the results from the simulation.

III. AB INITIO SIMULATION STUDY OF l -Ge

A. Simulation procedure

All calculations were performed with the Vienna Ab initio Simulation Package (VASP)^{30,31}, which is based on density functional theory. We carried out most simulations of l -Ge for an ensemble of 64 atoms in a cubic supercell with periodic boundary conditions. The simulated density was $\rho = 5.53 \text{ g/cm}^3$, which corresponds to a box of length 11.175 Å.

The atomic dynamics was described in the micro-

canonical (N, V, E) ensemble. Ultrasoft Vanderbilt pseudopotentials³² and the generalized gradient approximation (GGA) with the functional PW91 for the exchange-correlation energy were used. The Brillouin zone was sampled by a $3 \times 3 \times 3$ Monkhorst-Pack mesh of k -points³³. The wave functions were expanded in a basis of more than 32000 plane waves, corresponding to an energy cut-off of 139.2 eV. One MD run was performed in a cell containing 200 atoms for which the k -point grid contained only the gamma point.

The starting configurations for the *ab initio* simulations were generated from classical MD simulations using the Stillinger and Weber potential¹⁶. For this purpose, systems of 64 Ge atoms were equilibrated at the desired temperatures (three independent samples were extracted from a 50 ps run at high temperature (1700 K); these samples were then equilibrated at the desired temperature by velocity scaling during 10 ps).

After switching to the *ab initio* (N, V, E) MD, and an equilibration time of 5 ps, three runs of 30 ps using a time step of 3 fs were performed at three different temperatures corresponding to the liquid (1390 K, 1080 K) and supercooled (680 K) states, all at the same density. A similar simulation scheme was used to perform a liquid MD run at 1390 K for the cell containing 200 atoms, the NVE trajectory spanning 15 ps. Three independent configurations of the trajectory at 680 K were quenched at a cooling rate of 68 K/ps in order to obtain three amorphous configurations of the system.

B. Numerical results

The mean-squared displacement (MSD) of atoms is one of the dynamic quantities that allows to check whether the system is a liquid or not. The MSD is computed from the relation

$$\delta r^2(t) = \langle [\mathbf{r}_i(t) - \mathbf{r}_i(0)]^2 \rangle, \quad (1)$$

and allows the diffusion constant D to be determined via the Einstein relation :

$$D = \lim_{t \rightarrow \infty} \frac{\delta r^2(t)}{6t}. \quad (2)$$

In Fig. 3 we compare the values for D as obtained from the simulations with experimental data from Pavlov and Dobrokhotov³⁴. For T around 1400 K, very similar values of D are obtained from experiment and *ab initio* MD, while according to Ref. 18 classical MD overestimates D by a factor of 2, which indicates that from this point of view the *ab initio* calculation is indeed more accurate than simulations with classical force fields. Having performed liquid simulations at 3 temperatures, we are able to observe an Arrhenius behavior of the diffusion constant with an activation energy around 0.72 eV. This

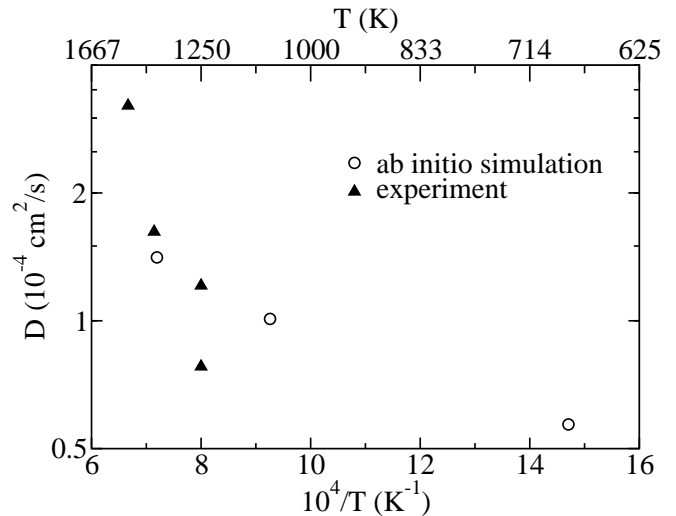


FIG. 3: Arrhenius plot of calculated and experimental diffusion constant D (experimental data from Ref. 34). Note that the vertical scale is logarithmic.

quantity corresponds to the average energy needed by a Ge atom to escape from its local environment and undergo diffusion and it is characteristic of a strong liquid.

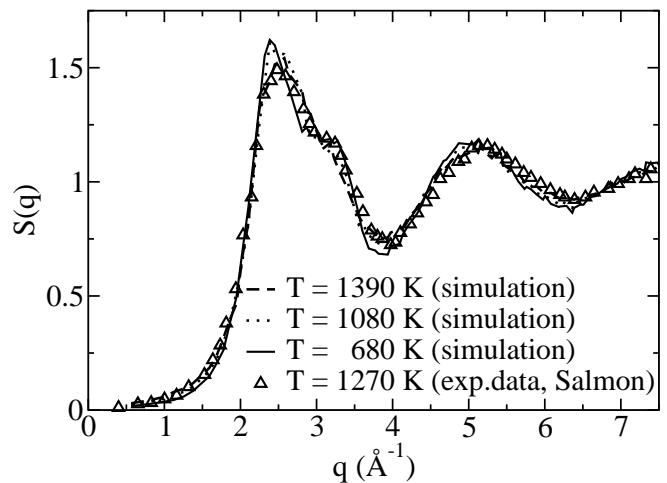


FIG. 4: Static structure factor of l -Ge: Simulated data for $T = 1390$ K (dashed line), $T = 1080$ K (dotted line), and $T = 680$ K (full line) and experimental data by Salmon¹⁰ at $T = 1270$ K (triangles).

The structure of the liquid can be characterized by the static structure factor which is defined as³⁵:

$$S(\mathbf{q}) = \frac{1}{N} \sum_{j=1}^N \sum_{l=1}^N \langle \exp(i\mathbf{q} \cdot (\mathbf{r}_j - \mathbf{r}_l)) \rangle. \quad (3)$$

It was computed using, at each temperature, 10000 atomistic configurations. The average is also performed over all \mathbf{q} vectors of the same magnitude. The results are

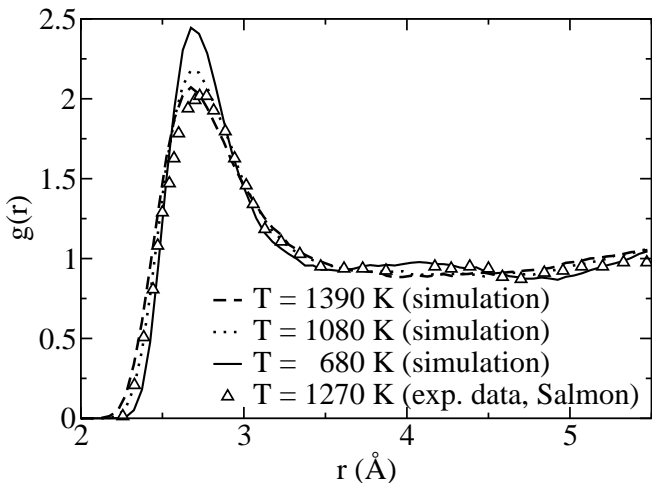


FIG. 5: Pair correlation function of *l*-Ge: Simulated data: $T = 1390$ K (dashed line); $T = 1080$ K (dotted line) and $T = 680$ K (full line) and neutron scattering data by Salmon¹⁰ at $T = 1270$ K (triangles).

shown in Fig. 4 together with the experimental result by Salmon¹⁰.

At $T = 1390$ K the main sharp peak occurs at $q = 2.53 \text{ \AA}^{-1}$ which is very close to the experimental values ($q_{max} \approx 2.50 \text{ \AA}^{-1}$)^{5,6,10}. At lower temperatures, the peak is shifted to slightly lower q values, which is consistent with measurements in the temperature range from 1270 K to 1820 K⁹. The characteristic feature of *l*-Ge shown by neutron diffraction studies⁹, the distinct shoulder at $q = 3.27 \text{ \AA}^{-1}$, i.e. on the high- q side of the first sharp peak, is reproduced well by the simulation. As T decreases, the height of the main peak increases and the shoulder becomes more distinct. These two features were described at higher temperatures in the simulation work by Kulkarni *et al.* who found that at $T = 2000$ K the shoulder disappears²⁴. The second peak of the static structure factor occurs at 5 \AA^{-1} which is slightly shifted from the experimental value reported by Salmon¹⁰ who found $q = 5.1 \text{ \AA}^{-1}$ (see also Waseda⁵), although the experimental value seems to have an uncertainty of $\approx 0.1 \text{ \AA}^{-1}$ ^{4,36}.

The pair correlation function $g(r)$, defined as³⁵

$$\rho g(\mathbf{r}) = \frac{1}{N} \sum_{i=1}^N \sum_{j \neq i}^N \langle \delta(\mathbf{r} - (\mathbf{r}_i - \mathbf{r}_j)) \rangle, \quad (4)$$

allows the structure of the system in real space to be characterised. A comparison of simulated and experimental $g(r)$ is given in Fig. 5. In particular we see that $g(r)$ hardly shows a second peak at distances beyond the first peak, in marked contrast to the situation found in simple liquids such as hard spheres. The structure of *l*-Ge is significantly different from that of simple liquids. In addition the height of the main peak increases with decreasing temperature but the structure at larger dis-

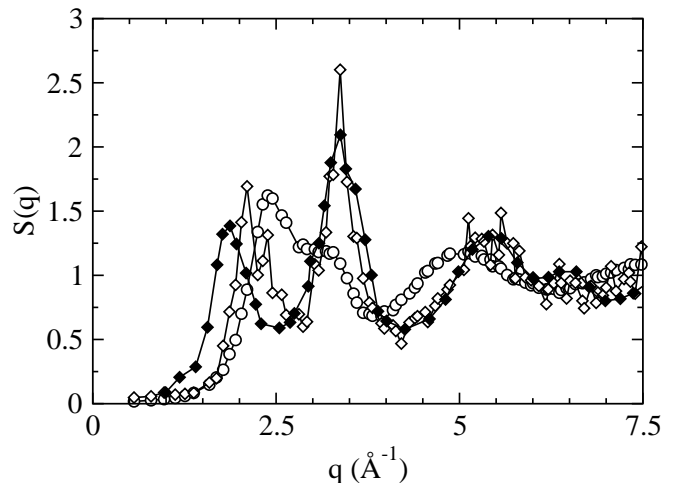


FIG. 6: $S(q)$ for supercooled and amorphous Ge: Comparison between simulation (supercooled state at $T = 680$ K (open circles) and amorphous state (open diamonds)) and experimental data, from Ref. 37, as obtained from neutron scattering with an amorphous sample (filled diamonds).

tances remains basically unchanged. Indeed both $S(q)$ and $g(r)$ show that structural changes over a wide range of temperatures from 680 to 1390 K are generally rather small.

Structural changes become more significant if the liquid phase is quenched to produce an amorphous phase. This can be seen in Fig. 6 in which we show $S(q)$ for the supercooled liquid at 680 K and the amorphous state. The amorphous phase was obtained by cooling down, over 10 ps and at constant volume, three independent configurations of the supercooled state at 680 K to $T = 0$ K. Thus for this state $S(q)$ was calculated by averaging over only three configurations, which is the reason for the substantial noise in the simulation data. In $S(q)$, the first peak is shifted to higher q reflecting the high, liquid density that we have imposed on the amorphous structure. At higher q , the agreement between experiment and simulation is much better. Looking at snapshots of the system in the amorphous state, one clearly sees a tetrahedral structure in which a Ge atom occupies the center of a tetrahedron. The calculated $g(r)$ for the amorphous state (not shown here) shows a main peak shifted to lower interatomic distances (as compared to the liquid state) while the intermediate peak near 4 \AA becomes much more pronounced, in agreement with experimental findings³⁷. The main peak in $g(r)$ corresponds to the interatomic distance between the center and a vertex of the tetrahedron while the higher interatomic distance at 4 \AA is associated with the distance between two vertices of the tetrahedron (see also Fig. 7). Despite imposing the higher liquid density on our amorphous structures, the shortest Ge-Ge distances are overestimated by several 0.1 \AA .

Given the nature of the many-body interactions in germanium and the resulting open structure, it is interesting

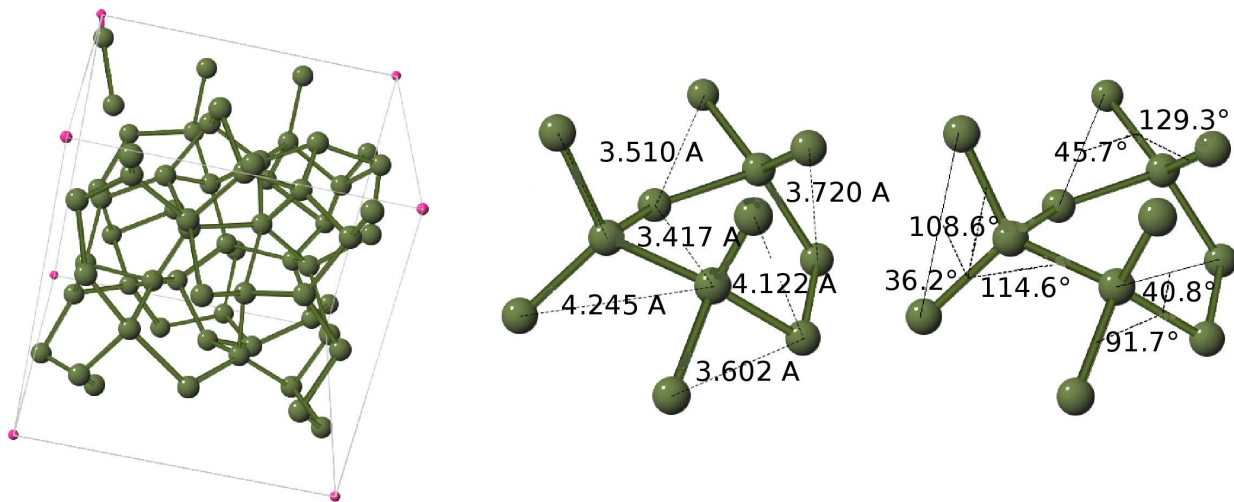


FIG. 7: (Color online) Calculated structure of amorphous Ge at $T = 0$ K. Left: Snapshot of the whole simulation box (with small spheres representing the corners of the box). Middle: Interatomic distances. Right: Bond angles.

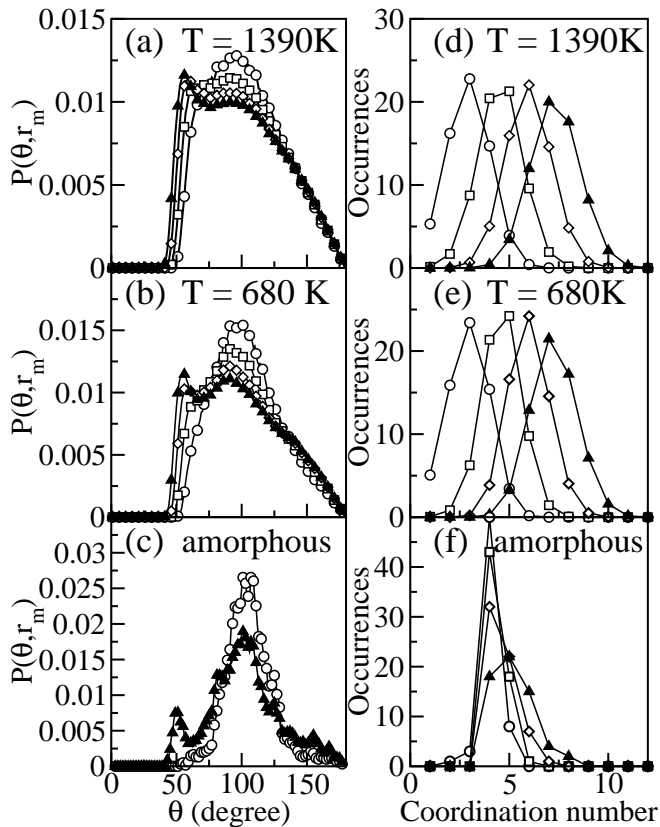


FIG. 8: Angular distribution (left) and coordination number (right) for liquid (top), supercooled (middle) and amorphous (bottom) phases of Ge for r_m in the vicinity of the first minimum of $g(r)$. Circles: $r_m = 2.8$ Å; Squares: $r_m = 3.0$ Å; Diamonds: $r_m = 3.2$ Å; Triangles $r_m = 3.4$ Å. The quantities for the liquid, supercooled, and amorphous phases are, respectively, averaged over 9000, 6300 and 3 configurations.

to compute the angular distribution of atoms. For this we define $P(\theta, r_m)$ as the normalized distribution of angles defined by vectors going from a reference atom i to two neighbors of i which are within a radius r_m of the reference atom. In Fig. 8 we show $P(\theta, r_m)$ for several values of r_m around the minimum in $g(r)$. In the liquid this minimum is not very pronounced, see Fig. 5, leading to an uncertainty regarding the definition of the nearest neighbor shell. In contrast, in the amorphous state, the first minimum in $g(r)$ (calculated, not shown here) is clearly defined allowing an unambiguous definition of nearest neighbors. We note that any bond angle distribution plot will tend to have a maximum close to 90° and that changes in the distribution as a function of radius and temperature are therefore particularly meaningful.

For liquid and supercooled systems, we observe a broad peak around $\theta = 98^\circ$ if $r_m = 2.8$ Å. With increasing r_m , this peak tends to shift to smaller angles, around $\theta = 90^\circ$. For the amorphous phase, the corresponding peak is observed at slightly larger angles, around 105° for $r_m = 2.8$ Å, indicative of a slightly more regular tetrahedral environment in the amorphous phase, even at higher pressure as imposed by the liquid density. With increasing r_m , a new peak appears for angles between 55° and 60° in the liquid and supercooled phases. At $T = 680$ K, this feature is more pronounced than at higher temperatures. In the amorphous phase, this peak appears at smaller angles, about 50° . A bond angle of 60° is characteristic of metallic bonding, since this value represents the locally most closely packed structure of the system. The broad peak around 100° is typical of flattened tetrahedra, the symmetric tetrahedral angle being 109.5° , see also Fig. 7.

Regarding the coordination number, most atoms have either 4 or 5 nearest neighbors in the amorphous phase (see right panels of Fig. 8). On the other hand, in the

liquid and supercooled phases, for typical values of the first minimum in $g(r)$, 3.4 Å, the coordination number is between 6 and 7.

We note that obviously the coordination number increases with increasing radius of the coordination sphere for both liquid and supercooled systems, which is consistent with the so-called β -tin hypothesis⁴. This hypothesis states that in l -Ge, each atom has four nearest neighbors on a flattened tetrahedron and two other neighbors slightly further away on the normal to the plane of the flattened tetrahedron (see Fig. 9 for a schematic representation of the local environment of β -tin). Denoting by r_0 the main interatomic distance reported from $g(r)$, i.e. $r_0 \simeq 2.5$ Å, the β -tin configuration would lead to interatomic distances of the order of r_0 (between the center and a vertex of the tetrahedron), $\sqrt{2}r_0 \simeq 3.53$ Å (between two adjacent vertices of the tetrahedron), and $2r_0 \simeq 5$ Å (between two opposite vertices of the tetrahedron) together with distances slightly higher than r_0 associated with the two further neighbors.

Snapshots of the simulated structure of amorphous Ge are shown in Fig. 7. On the left, the 64 atoms are represented together with the corners of the simulation box. The bonds between atoms correspond to two covalent radii (1.22 Å for Ge) plus a bond tolerance of 0.4 Å so a bond is drawn for interatomic distances smaller than 2.84 Å. The two other plots show a zoom into this structure. Three “tetrahedra” are represented together with some interatomic distances and bond angles. The covalent bond length of Ge corresponds to the main peak in $g(r)$ around 2.5 Å. On the other hand, the distance between two neighboring vertices of a tetrahedron ranges from 3.5 Å to 4.5 Å, which accounts for the broad peak around 4 Å in $g(r)$ (calculated, not shown here). Looking at the bond angles, their values are mainly distributed between 85° and 130° with an average value of 105°, close to the tetrahedral value (see Fig. 8). At higher interatomic distances (see distribution for $r_m = 3.4$ Å in Fig. 8), another peak appears around 50°. This one is due to the angles formed by the two following vectors: The first one goes from a vertex to the center of the tetrahedron while the second one goes from the same initial vertex to another vertex of the same tetrahedron. This is also shown in Fig. 7.

Having established that the liquid simulations do indeed describe well the corresponding experimental system and having studied the structural aspects, we now investigate the dynamic features of the system. For this we start with the intermediate scattering function which is defined as³⁵

$$F(\mathbf{q}, t) = \frac{1}{N} \sum_{j=1}^N \sum_{k=1}^N \langle \exp[i\mathbf{q} \cdot (\mathbf{r}_j(t) - \mathbf{r}_k(0))] \rangle \quad (5)$$

Since the system is isotropic, we have performed an average over the different orientations of \mathbf{q} .

Figure 10 shows the (normalized) $F(q, t)$ of l -Ge at 1390 K and for low q values from the large simulation

cell. The oscillations are associated with the presence of the acoustic mode at these wave-vectors. The period of these oscillations decreases with increasing q and also they become more damped, which is directly associated with the shape of the dispersion and damping of the acoustic phonon as a function of q , as will be discussed in more detail below.

The dynamic structure factor $S(q, \omega)$ was computed by a Fourier transform in time of $F(q, t)$ ³⁵. In a periodic system of cell side L only the reciprocal lattice points $(n_x, n_y, n_z) \cdot 2\pi/L$ are accessible. The first q -point corresponds to a spatial correlation over a distance L , which is not meaningful in a cell of side L . q -points bigger than $4\pi/L$ correspond to correlations over distances shorter than $L/2$, which are uniquely defined. In the intermediate range there is a progressive increase in meaningful correlations which correspond to distances between atoms close to the centre and those close to the apexes of the cell. The lowest unambiguous q -values, calculated in 0.1 \AA^{-1} q -strips, for the 200 atom cell start at 0.7 \AA^{-1} and at 1.1 \AA^{-1} for the 64 atom cell. At smaller q , $q \leq 1 \text{ \AA}^{-1}$, $S(q, \omega)$ shows a well defined acoustic mode, the position of which can be compared directly with the corresponding experimental results from the inelastic X-ray scattering of Ref. 11. Such a comparison is made in Fig. 11 and it shows a very good agreement between experiment and simulations. The width of the acoustic phonons increases with frequency, both in the experiment and in our simulations. At 1.2 \AA^{-1} the phonons are hardly visible in the experimental spectrum and in the simulations, the width is of the same order as the frequency. Accordingly we estimate the error in the frequency to be a few meV. We also mention that the dispersion of the acoustic mode does not show any significant variation with T in the temperature range investigated.

At higher q values, $q > 1 \text{ \AA}^{-1}$, the QENS signal dominates $S(q, \omega)$ (see Fig. 12). Fitting the quasi-elastic line of $S(q, \omega)$ with a Lorentzian allows to determine its half-width at half maximum (HWHM), the q -dependence of which is shown in Fig. 13 together with the corresponding structure factor. Unconstrained fits of the Focus data lead to an underestimation of the spectral width at low q ($< 1.8 \text{ \AA}^{-1}$), where the QENS intensity is weak, and also at higher q ($> 3.2 \text{ \AA}^{-1}$), where only the negative energy transfer part of the spectrum is present, and therefore we show the Focus data only for $1.8 \text{ \AA}^{-1} \leq q \leq 3.2 \text{ \AA}^{-1}$. The simulated widths are obtained from the simulation at 1390 K by fitting $S(q, \omega)$ with a Lorentzian. From Fig. 13 we recognize that the data from the simulation agrees very well with the one from the experiment. In particular we see that in the simulation as well as in the experiments a narrowing of the quasi-elastic peak is observed for $q = 2.4 \text{ \AA}^{-1}$ and between $q = 2.8 \text{ \AA}^{-1}$ and 3.2 \AA^{-1} , which corresponds to the main peak and the shoulder in the static structure factor, respectively (see line in Fig. 13). This behavior can be interpreted as de Gennes narrowing¹³, i.e. the fact that if one considers the dynamics on length-scales that are close to the one

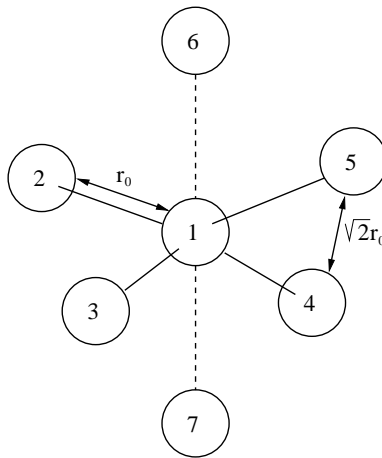


FIG. 9: Schematic representation of the β -tin configuration. Atom 1 is at the center of the flattened tetrahedron formed by atoms 2, 3, 4, and 5. Atoms 6 and 7 are the second nearest neighbors. Distances are: $d_{12} = d_{13} = d_{14} = d_{15} \approx r_0$; $d_{23} = d_{34} = d_{45} = d_{52} \approx \sqrt{2}r_0$; $d_{24} = d_{35} \approx 2r_0$.

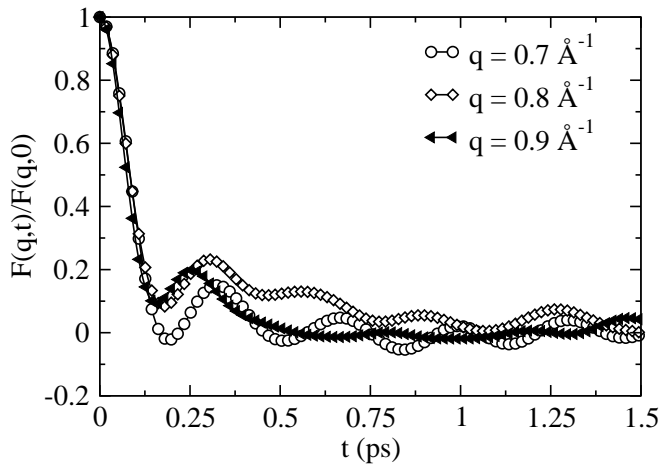


FIG. 10: Collective dynamic properties of l -Ge at low q values: Simulated intermediate scattering function $F(q, t)$ at $T = 1390$ K normalized by its value at $t = 0$.

of the local structure of the liquid, the structure is basically preserved and thus there is only a relatively small loss of memory and consequently a small broadening of the dynamic structure factor.

The q -dependence of the width of the quasi-elastic peak can be compared with theoretical predictions based on different models. The simplest expression for the HWHM for a dense monoatomic liquid is that the half-width ω_q is the square root of the normalized second frequency moment³⁵:

$$\langle \omega_q^2 \rangle = \frac{k_B T}{m S(q)} q^2. \quad (6)$$

In a somewhat refined approach, Cohen *et al.*¹⁴ predicted for a dense hard-sphere fluid the half-width ω_h to be given by

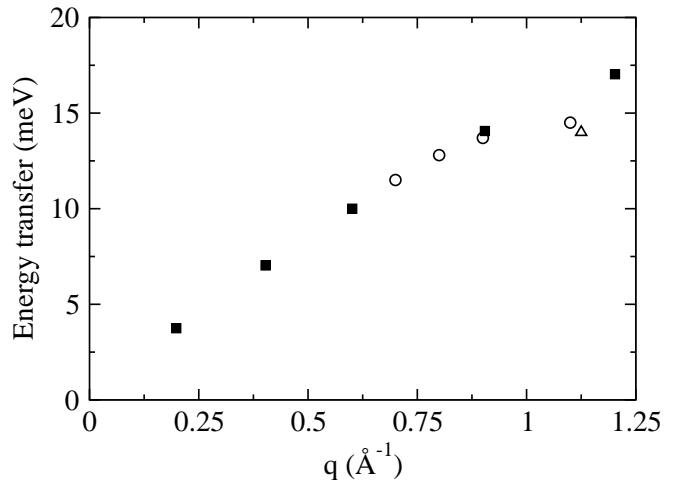


FIG. 11: Dispersion of the frequency of the acoustic phonon as a function of q : Comparison between inelastic X-ray scattering data at $T = 1250$ K from Ref. 11 (squares) and simulation at $T = 1390$ K (circles for the 200 atom cell, triangles for the 64 atom cell).

$$\omega_h(q) = \frac{D_E q^2}{S(q)} d(q), \quad (7)$$

where

$$d(q) = [1 - j_0(q\sigma) + 2j_2(q\sigma)]^{-1}. \quad (8)$$

Here D_E is the self-diffusion coefficient of the hard-sphere fluid within the Enskog theory, σ is the diameter of the hard spheres, and $j_0(x)$ and $j_2(x)$ are the zeroth- and second-order spherical Bessel functions, respectively. Note that equation (7) is only valid for intermediate values of q , $1 < q\sigma < \sigma/l$, where $\sigma/l \gg 1$ with l the mean free path of a particle which, since we are considering a

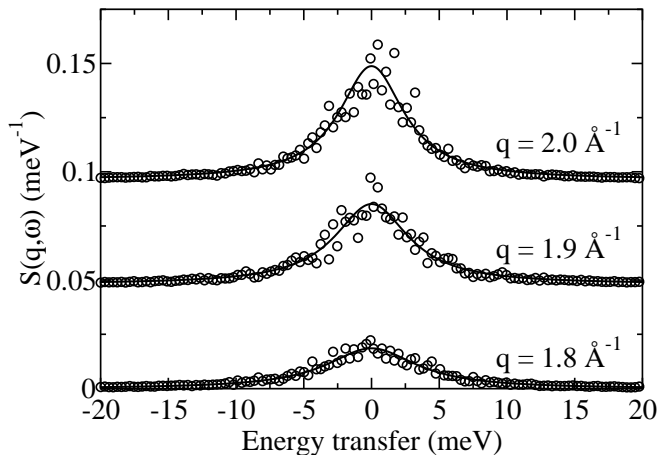


FIG. 12: Simulated dynamic structure factor for l -Ge at 1390 K for different q values (Symbols: Simulation; Line: Fit with a Lorentzian).

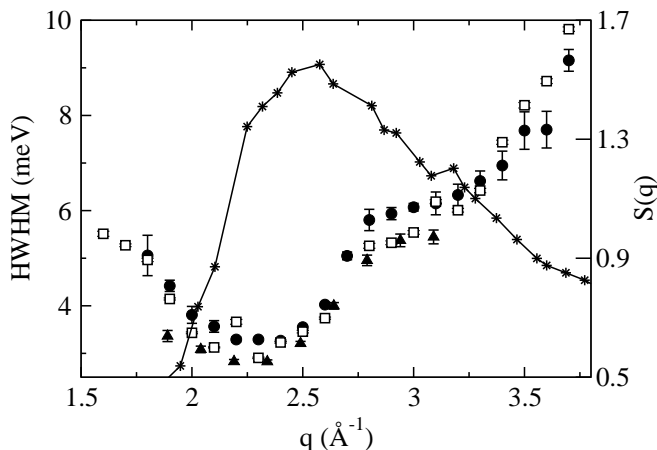


FIG. 13: Half width at half maximum of $S(q, \omega)$ as a function of q together with the static structure factor. Circles: Triple-axis measurements (4F1); Triangles: Time-of-flight measurements (Focus); Squares: Simulation; Stars and straight line: Simulated $S(q)$ at 1390 K.

dense system, is much smaller than σ . Approximating the Ge liquid by a system of hard spheres, we have calculated the quantity $\omega_h(q)$ by using the static structure factor from the AIMD simulations at 680 K and 1390 K. For the size of the hard spheres, the location of the first peak in the pair correlation function gives, see Fig. 5, $\sigma = 2.8 \text{ \AA}$ at $T = 1390 \text{ K}$ and $\sigma = 2.7 \text{ \AA}$ for $T = 680 \text{ K}$. For D_E , we used the value of the self-diffusion constant D calculated from the simulation (its dependence on the mass and the density can be expected to be very similar to that of the self-diffusion constant of the Enskog theory).

These models are compared with the width of the quasi-elastic signal obtained from AIMD in Fig. 14. Both models show de Gennes narrowing at $q = 2.3 \text{ \AA}^{-1}$. For the dense monoatomic fluid model, the q -dependence of

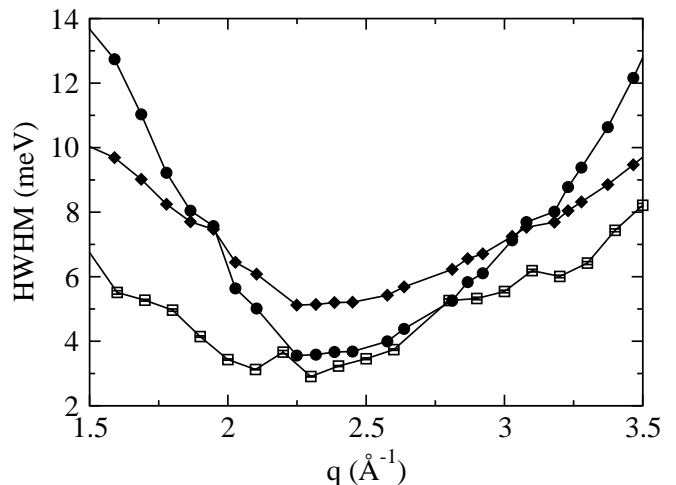


FIG. 14: Half width at half maximum of the dynamic structure factor as a function of q for $T = 1390 \text{ K}$. Squares: Simulation; Diamonds: Second frequency moment ω_q of a monoatomic liquid, see Eq. (6); Circles: ω_h as calculated from the theory of dense hard-sphere fluids, see Eq. (7).

ω_q is reasonably good but the value of ω_q is generally overestimated by a factor of 2. Such a systematic discrepancy has also been found for a variety of *simple* liquids (Ar, Kr, Lennard-Jones)¹⁴ and thus it is not surprising that in the present system, which has a much more complex structure, we find a similar deviation. In contrast to this the width ω_h predicted by the hard sphere model is in better agreement close to $q = 2.3 \text{ \AA}^{-1}$ but the increase in width away from this q -value is overestimated. Also this result is in qualitative agreement with the ones reported by Cohen *et al.* for simple liquids¹⁴ which thus gives evidence that Eq. 7 is not valid for simple liquids and for network forming systems.

IV. DISCUSSION AND CONCLUSION

Liquid Ge is a system of fundamental interest for its structure and fluctuations. Accordingly a number of models have been proposed to describe the local structure of this liquid. Due to the complexity of the system, models can only be validated by comparison with experimental data but it is found that static structure measurements presently available are not sufficient to distinguish between various plausible models. Since the local structure of a liquid is time dependent, a more stringent requirement of any model is that the structural fluctuations should also be correctly reproduced. In this context, we have presented new QENS measurements of the diffusive dynamics of Ge on the length scale of $\sim 3 \text{ \AA}$, which is most pertinent to the structural issues on the scale of the nearest neighbor distance.

To understand this new QENS data, we have also performed *ab initio* simulations of liquid and amorphous Ge, the latter highlighting features of the liquid phase. These

simulations not only reproduce accurately the quasi-elastic broadening but also IXS data of acoustic phonons at small q , which concerns the structure on a length scale $> 6 \text{ \AA}$. In addition, we have found very good agreement for the static structure factor, the pair correlation function and the diffusion constant, the latter enabling an activation energy of 0.7 eV to be determined for diffusion processes, which is characteristic of a strong liquid.

The success of AIMD is in contrast to classical MD simulations that use two and three body potentials that, although they reproduce reasonably well the average structural properties, do not give an accurate description of the dynamics^{17,38}. The QENS data and simulations also allow theoretical models, which relate the spectral line width to the static structure factor, to be tested. We have found that the second frequency moment given by Eq. (6) does not give a good description of the line width in the whole q -range whereas expression (7) describes this width well around the main peak in the static structure factor.

Simulations also allow models to be investigated at the atomic level. Analysing the AIMD trajectories shows an average coordination number of 6-7 for the liquid and a broad range of bond angles with an average value of 100 degrees. In contrast to this, for amorphous Ge, the

coordination number is close to 4 and the average bond angle is closer to the value for a symmetric tetrahedron, even when the liquid density is imposed. In terms of simple models of the structure, the AIMD simulation is approximately consistent with the β -tin hypothesis⁴.

In conclusion, QENS data constitutes experimental evidence that can differentiate between different theoretical and numerical models. The *ab initio* model presented here is in very good agreement with all new and existing, structural and dynamic experimental data. Further details of the liquid structure are most likely to be obtained from more in-depth investigation of the MD trajectories.

Acknowledgments

The authors thank R. Bellissent (CEA, Grenoble) for useful discussions in designing the sample cell and preparing the experiments and P. Martin (ILL) for his help in preparing the niobium cell. Some of the calculations were performed on the CCRT/CEA clusters. Part of this work was supported by the European Community's Human Potential Program under contract HPRN-CT-2002-00307, DYGLAGEMEM.

* Present address: Unité de Recherche Biopolymères, Interactions, Assemblages, INRA, BP 71627, 44316 Nantes cedex 3, France; Email: virginie.hugouvieux@nantes.inra.fr

¹ Y.K. Vohra, K.E. Brister, S. Desgreniers, A.L. Ruoff, K.J. Chang and M.L. Cohen, *Phys. Rev. Lett.* **56**, 1944 (1986).
² P.M. Glazov, S.N. Chizhevskaya and N.N. Glagoleva, *Liquid Semiconductors* (Plenum, New York, 1969), Chap. 3.
³ A. Filippini and A. Di Cicco, *Phys. Rev. B* **51**, 12322 (1995).
⁴ S.P. Isherwood, B.R. Orton and R. Mănăilă, *J. Non-Cryst. Solids* **8-10**, 691 (1972).
⁵ Y. Waseda and K. Suzuki, *Zeit. Phys. B* **20**, 339 (1975).
⁶ M.-C. Bellissent-Funel and R. Bellissent, *J. Non-Cryst. Solids* **65**, 383 (1984).
⁷ M. Davidović, M. Stojić and D. Jović, *J. Phys. C: Solid State Phys.* **16**, 2053 (1983).
⁸ J.P. Gabathuler and S. Steeb, *Z. Naturforsch.* **34a**, 1314 (1979).
⁹ Y. Kawakita, S. Takeda, T. Enosaki, K. Oshima, H. Aoki, T. Masaki and T. Itami, *J. Phys. Soc. Jpn* **71**, 12 (2002).
¹⁰ P.S. Salmon, *J. Phys. F: Met. Physics* **18**, 2345 (1988).
¹¹ S. Hosokawa, Y. Kawakita, W.C. Pilgrim and H. Sinn, *Phys. Rev. B* **63**, 134205 (2001).
¹² N. Yoshimoto, H. Shibata, M. Yoshizawa, K. Suzuki, K. Shigematsu and S. Kimura, *Jpn. J. Appl. Phys.* **35**, 2754 (1996).
¹³ P.G. de Gennes, *Physica* **25**, 825 (1959).
¹⁴ E. G. D. Cohen, P. Westerhuijs and I.M. de Schepper, *Phys. Rev. Lett.* **59**, 2872 (1987).
¹⁵ N.W. Ashcroft, *Nuovo Cimento D* **12**, 597 (1990).
¹⁶ F.H. Stillinger and T.A. Weber, *Phys. Rev. B* **31**, 5262

(1985).
¹⁷ K. Ding and H.C. Andersen, *Phys. Rev. B* **34**, 6987 (1986).
¹⁸ W. Yu, Z.Q. Wang and D. Stroud, *Phys. Rev. B* **54**, 13946 (1996).
¹⁹ G. Kresse and J. Hafner, *Phys. Rev. B* **47**, 558 (1993).
²⁰ G. Kresse and J. Hafner, *Phys. Rev. B* **49**, 14251 (1994).
²¹ N. Takeuchi and I.L. Garzon, *Phys. Rev. B* **50**, 8342 (1994).
²² R. Car and M. Parrinello, *Phys. Rev. Lett.* **55**, 2471 (1985).
²³ V. Godlevsky, J.R. Chelikowsky and N. Troullier, *Phys. Rev. B* **52**, 13281 (1995).
²⁴ R.V. Kulkarni, W.G. Aulbur and D. Stroud, *Phys. Rev. B* **55**, 6896 (1997).
²⁵ J.D. Chai, D. Stroud, J. Hafner and G. Kresse, *Phys. Rev. B* **67**, 104205 (2003).
²⁶ S. Janssen, J. Mesot, L. Holitzner, A. Furrer and R. Hempelmann, *Physica B* **234**, 1174 (1997).
²⁷ S. Janssen, D. Rubio-Temprano and A. Furrer, *Physica B* **283**, 355 (2000).
²⁸ <http://sinq.web.psi.ch/sinq/instr/focus/focus.html>
²⁹ <http://www-llb.cea.fr/spectros/pdf/4f1-llb.pdf>
³⁰ G. Kresse and J. Furthmüller, *Phys. Rev. B* **54**, 11169 (1996).
³¹ G. Kresse and J. Furthmüller, *Comput. Mater. Sci.* **6**, 15 (1996).
³² D. Vanderbilt, *Phys. Rev. B* **41**, 7892 (1990).
³³ H.J. Monkhorst and J.D. Pack, *Phys. Rev. B* **13**, 5188 (1976).
³⁴ P.V. Pavlov and E.V. Dobrokhotov, *Sov. Phys. Solid State* **12**, 225 (1970).
³⁵ J.-P. Hansen and I.R. McDonald, *Theory of simple liquids* (Academic Press, 2006).

- ³⁶ B.R. Orton and S.P. Woodisse, *J. Phys. F: Met. Physics* **3**, 1141 (1973).
- ³⁷ G. Etherington, A.C. Wright, J.T. Wenzel, J.C. Dore, J.H. Clarke and R.N. Sinclair, *J. Non-Cryst. Solids* **48**, 265 (1982).
- ³⁸ V. Hugouvioux, *A complete simulation of neutron scattering experiments: From model systems to liquid germanium* (PhD Thesis, Université Montpellier II, 2004).